made clear in the introduction – this means that not only should the problem you study be presented but its historical background, its relevance to science and technology, the specific phenomena it can be used to describe or investigate, and the outstanding open issues related to it should be explained. Failure to achieve this could disqualify the paper.

Review Procedures

All papers will undergo a thorough peer review unless the Editor notes at once that the subject matter of the paper is not appropriate for the journal; in this case, it will be returned promptly to the author. Every effort will be made to secure a decision about the paper in 2–3 months and to publish accepted papers within a year of submission.

Manuscript Preparation

Standard manuscript format is requested: double-spaced type, preferably on 8½ by 11 paper, and ample margins.

Title page—The title should be brief, descriptive, and appropriate for indexing. Each author's name and affiliation should be listed.

Abbreviated title—On the bottom of the title page, list the essence of the title using no more than 50 characters for use as a running head.

Abstract—Provide an abstract that summarizes what was studied, the main results, and the conclusions stemming from those results. The abstract should not exceed a double-spaced typed page. Because abstracts are reproduced in abstracting and indexing services, abbreviations should not be used, mathematical formulas should be kept to a minimum, and bibliographic citations should be written out in full.

Abbreviations—Define abbreviations when they first occur in the text and then use only the abbreviation.

References—List the references on a separate sheet of paper and double-space throughout. Authors may use their own style of referencing, including style of citations in text, provided it is consistent and sensible. References must include the author(s), title, correct journal or series name when applicable, publisher, and place and date of publication. Please provide complete and accurate information; if a reader cannot locate the reference in less than three hours with the information you provide, your referencing is a sterile exercise at best.

Acknowledgments—Technical assistance, advice, etc. should be acknowledged in a separate section at the end of the text before the references.

Tables—Number tables consecutively in order of appearance. Each table must have a caption typed above the tabular material. Symbols and abbreviated units of measure referred to in the table must be explained in the caption. All tables must be cited in the text. Please use as few horizontal and vertical lines in the body of the table as possible.

Illustrations—Illustrations should be of professional quality, *including* the labeling. All illustrations must have legends; they should be double-spaced on a separate sheet and included with the manuscript. Symbols and abbreviated units of measure appearing in an illustration must be explained in the legend. All illustrations must be cited in the text. Line drawings can be submitted on plain, good-quality paper; please indicate if you have sent the originals. Photocopies are not acceptable. The preferred form for halftones is 5 by 7 unmounted, glossy photographs. Color art can be reproduced only if the author bears the cost; the preferred form is slides. If you have unusual requirements for your artwork, please contact the journal editorial office. Previously published illustrations must be accompanied by written permission from the author and publisher.

Mathematical Notation

Authors should provide a key to unusual or complex notation. All variables will be set in italic type and should not be marked; underbars written or typed in black under a variable will be reproduced as underbars and not italic. Unusual symbols, Greek, German, script, roman, and open letters should be clearly labeled. To indicate boldface, a wavy black line should be marked under the variable(s), (e.g., a)—be sure that it is clear that you intend boldface and not an italic variable with an undertilde. Do not double-strike to indicate boldface. Please clarify the following: product and summation signs versus the Greek letters, null set versus phi, oh versus zero, lowercase x versus multiplication sign, one versus ell, prime versus superscript one, and capital versus lowercase letters.

Offprints

Twenty-five offprints will be provided with each article to the principal author (considered to be the author who is mailed the page proofs for correction). He or she can order additional copies using a form provided with the proofs.

TEX Papers

Submission of papers in TEX is greatly encouraged; papers thus submitted will be given priority of publication when possible. Macros for preparation of manuscripts with documentation are available in Plain TEX, LaTEX, and AMS-TEX and can be obtained via e-mail: netlib@research.att.com. Specify as follows: send index from typesetting/springer.

The following formats are accepted: 5.25" diskette MS-DOS, 3.5" diskette MS-DOS, 3.5" diskette Apple Macintosh UNIX ¼ inch, and 8 mm tape. *Please submit hard copy of the final version of your paper together with your diskette or tape.* The latter should contain your source file and the final DVI file. If you use additional macros please be sure to include them in the beginning of your file so that our typesetter will be able to make any needed corrections. Line art can be included in the file if it is produced in TEX or Postscript; however, *please send a hard copy of your figures* as well.

Do not forget to include a guide to unusual or complex notation and to mark any ambiguous variables even though you have used TEX.

J. Nonlinear Sci. Vol. 4: pp. 315–328 (1994)

Journal of Nonlinear Science

Truncated Fractal Basin Boundaries in the Pendulum with Nonperiodic Forcing

I. Dobson [1] and D. F. Delchamps [2]

[1] Department of Electrical and Computer Engineering, University of Wisconsin, Madison, WI 53706, USA

[2] School of Electrical Engineering, Cornell University, Ithaca, NY 14853, USA

Received November 12, 1991; revised version accepted August 17, 1993
Communicated by Stephen Wiggins

Summary. It is well known that oscillators such as the pendulum can have fractal basin boundaries when they are periodically forced with the consequence that the long term behavior of the system may be unpredictable. In engineering and physical applications, the forcing is often nonperiodic and eventually decays to zero, and simulation of the pendulum with decaying forcing (M. Varghese, J. S. Thorp, Physical Review Letters, vol. 60, no. 8, pp. 665–668, Feb. 1988) exhibits truncated fractal basin boundaries which also limit the system predictability. We develop a coordinate change for the pendulum with decaying forcing that allows us to apply standard qualitative methods to study the basin boundaries. We prove that the basin boundaries cannot be fractal and show by example how the extreme stretching and folding leading to a truncated fractal basin boundary may arise.

Key words. basin boundary, fractal, pendulum, stable manifold

1. Introduction

Many important problems in engineering and physics can be modeled as dynamical systems with multiple stable equilibria. Solution trajectories of a given system are generally attracted to one of the stable equilibria, and an initial condition giving rise to such a trajectory is said to be in the *basin of attraction* of that equilibrium. Thus one can specify the long term system behavior by describing the various basins of attraction in state space. The basins are separated from each other by basin boundaries; describing the basin boundaries is equivalent to describing the basins and the long term behavior. For some systems, the basin boundaries are mildly deformed hyperplanes of dimension one less than the state space and divide the state space into basins in a straightforward way. For example, consider the vector field X of the unforced, damped pendulum:

$$(\dot{\theta}, \dot{v}) = X(\theta, v) = (v, -\sin\theta - dv), \quad (\theta, v) \in \mathbb{R}^2. \tag{1}$$

X has 2π-periodicity in the angle coordinate and stable equilibria (sinks) at $(2n\pi, 0)$, $n \in \mathbf{Z}$, along with saddles at $((2n+1)\pi, 0)$, $n \in \mathbf{Z}$. The basins of $(2n\pi, 0)$, $n \in \mathbf{Z}$, are open sets in $\mathbb{R}^2$ and are separated by the stable manifolds W_n^s of the saddles $((2n+1)\pi, 0)$, $n \in \mathbf{Z}$ (see Figure 1). (The *stable manifold* (*unstable manifold*) of an equilibrium is the set of initial conditions tending to that equilibrium under the flow of X as time tends to ∞ $(-\infty)$ (Guckenheimer and Holmes 1986). The stable manifold of a sink is the same as its basin of attraction.) W_n^s, $n \in \mathbf{Z}$, are the basin boundaries, and each W_n^s is a smooth curve dividing $\mathbb{R}^2$ into two parts.

Nonetheless, simple systems can have surprisingly complicated basin boundaries. For example, when oscillators such as the pendulum or Duffing's equation are forced periodically, the boundaries separating the basins of attraction of stable periodic orbits can be fractal. The infinitely fine fractal structure makes it impossible to determine the basin boundary with a finite precision technique such as numerical integration on a computer, and numerical prediction of long term system behavior is fundamentally limited (Grebogi et al. 1983; McDonald et al. 1985).

Basin boundaries in oscillators with periodic forcing have been studied by several authors, e.g., Gwinn and Westervelt (1985), Moon and Li (1985), Hockett and Holmes (1986), Grebogi et al. (1987), Hammel and Jones (1989), Dobson (1989b). However in many engineering applications, the forcing is intended to model either a disturbance that eventually decays to zero or some other part of the system whose effect vanishes asymptotically because of its damping. See Varghese and Thorp (1988b) for an application to large scale electric power systems. Varghese and Thorp (1988a) studied the pendulum with exponentially decaying sinusoidal forcing $ge^{-\alpha t}\cos\omega t$ and showed numerically that the boundaries between basins of attraction were truncated fractals. That is, the basin boundaries exhibited self-similar structure for only a finite number of enlargements. (True fractals exhibit self-similar structure for any number of enlargements.) Truncated fractal basin boundaries can be seen under a sufficiently large number of enlargements to have a simple structure, but are effectively fractal for fewer

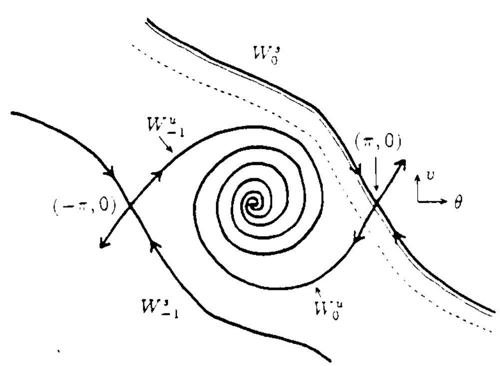

Fig. 1. A small impulse.

enlargements. We expect truncated fractal basin boundaries to be more common in applications than the more idealized case of true fractals and to cause for practical purposes a similar obstruction to estimating the long term system behavior.

In this paper we consider the forced, damped pendulum suspended in time:

$$(\dot{\theta}, \dot{v}, \dot{t}) = (v, -\sin\theta - dv + f(t), 1), \qquad (\theta, v, t) \in \mathbb{R}^3, \tag{2}$$

where the forcing function f is smooth and f and f' have norms asymptotically bounded by an exponential decay. That is, there are positive constants K, α, S such that

$$|f(t)| \le Ke^{-\alpha t} \quad \text{and} \quad |f'(t)| \le Ke^{-\alpha t} \quad \text{for } t \ge S. \tag{3}$$

This is a very general class of forcing functions that includes forcing of the form $f(t) = ge^{-\alpha t}\cos\omega t$ used in Varghese and Thorp (1988a). In (2), the dots denote differentiation with respect to the independent time variable τ and t denotes the third component of the state vector. We assume that the damping $d > 0$. Vector field (2) has no equilibria, but since the forcing eventually dies away, we generally expect the (θ, v) coordinates of solutions to approach asymptotically one of the stable equilibria $(2n\pi, 0)$, $n \in \mathbf{Z}$, of the unforced pendulum (1). By analogy with (1), we expect 3-dimensional basins of attraction of the "asymptotic equilibria" to be separated by smooth 2-dimensional boundaries. The purpose of this paper is to prove these assertions and to try to describe the basin boundaries qualitatively so that the way in which the forcing affects the asymptotic behavior of (2) may be better understood. In particular, we prove that the basin boundary is not fractal and show by examples how the truncated fractal structure of the basin boundary can arise. One of the examples is an impulsively forced pendulum in which extreme stretching and folding of the basin boundary can be demonstrated by elementary methods. Previous versions of this paper appeared in Dobson and Delchamps (1989) and Dobson (1989a).

Techniques such as Poincaré maps that are useful in analyzing periodically forced pendulums depend crucially on the periodicity of the forcing and seem quite useless for analyzing pendulums with decaying forcing. The pendulums with decaying forcing are simpler in that they tend to unforced pendulums as time tends to infinity and the forcing dies away. However there are no equilibria in bounded regions of state space. This paper develops a coordinate transformation for (2) that yields a C^1 vector field $\tilde{X}$ whose equilibria coincide with those of the unforced pendulum and for which "time infinity" occurs in the middle of the 3-dimensional state space. The existence of the equilibria and the C^1 smoothness of $\tilde{X}$ allow the analysis to proceed along conventional lines. In particular, the stable manifold theorem can be applied to construct a basin boundary rigorously. Our reformulation of (2), although obvious once stated, is central to the subsequent development.

An alternative way to construct the basin boundary sketched in Section 5 assumes that the forcing f is small and uses the hyperbolicity of the saddle type orbits to deduce the persistence of stable manifolds. This type of result for nonautonomous systems is developed much further in Lerman and Shil'nikov (1992) to study perturbations of homoclinic structures.

2. A Coordinate Change

We change the t coordinate of the state space of (2) according to the smooth transformation

$$r = e^{-\alpha t/2} \quad \text{or} \quad t = -2\alpha^{-1} \ln r. \tag{4}$$

(Recall that $\alpha > 0$ controls the rate of decay of f and f' according to (3).) In (θ, v, r) coordinates the state space becomes $\mathbb{R}^2 \times (0, \infty)$ and (2) becomes

$$(\dot\theta, \dot v, \dot r) = (v, -\sin\theta - dv + f(-2\alpha^{-1}\ln r), -\alpha r/2). \tag{5}$$

Define $h : \mathbb{R} \to \mathbb{R}$ by

$$h(r) = \begin{cases} f(-2\alpha^{-1}\ln|r|), & r \neq 0, \\ 0, & r = 0, \end{cases} \tag{6}$$

h is a C^1 function since $|h(r)| \leq Ke^{-\alpha t} = Kr^2$ and $|h'(r)| \leq 2\alpha^{-1}K|r|$ for $|r| \leq e^{-\alpha S/2}$. The vector field (5) on $\mathbb{R}^2 \times (0, \infty)$ is then "contained" in the following vector field $\tilde X$ on $\mathbb{R}^2 \times \mathbb{R}$:

$$(\dot\theta, \dot v, \dot r) = \tilde X(\theta, v, r) = (v, -\sin\theta - dv + h(r), -\alpha r/2). \tag{7}$$

Since h is C^1, $\tilde X$ is a C^1 vector field. Note that $\tilde X$ need not be C^2; any function $f(t)$ that behaves like $e^{-\alpha t}\cos\omega t$ for large t yields a function h and a vector field $\tilde X$ that are not C^2 at $r = 0$.

It is convenient to write $\Sigma_{r=k} = \{(\theta, v, r) | r = k, \ (\theta, v) \in \mathbb{R}^2\}$ for the plane of constant r in the state space of (7). For $k \neq 0$, $\Sigma_{r=k}$ corresponds to a plane of constant t in the state space of (2) that we write as $\Sigma_{t=\tau}$. Note, for example, that $\Sigma_{r=1}$ corresponds to $\Sigma_{t=0}$ and that $\Sigma_{r=0}$ can be thought of as corresponding to $\Sigma_{t=\infty}$. $\Sigma_{r=0}$ is an invariant plane of (7) containing the system equilibria and the vector field $\tilde X$ on $\Sigma_{r=0}$ is identical to the vector field X of the unforced pendulum (1).

We study the behavior of (2) by studying $\tilde X$. $\tilde X$ has sinks at $(2n\pi, 0, 0)$ and type one hyperbolic equilibria at $((2n+1)\pi, 0, 0)$, $n \in \mathbf{Z}$. Since $\tilde X$ is C^1 and the equilibria are hyperbolic, the stable manifold theorem (Palis and de Melo 1982) can be applied. For each n, the sink at $(2n\pi, 0, 0)$ has a 3-dimensional basin of attraction and the equilibrium at $((2n+1)\pi, 0, 0)$ has a 2-dimensional C^1 stable manifold $\tilde W_n^s$. $\tilde W_n^s$ is an immersed submanifold of the state space. The asymptotic behavior of initial conditions of vector fields (2) and (6) correspond under the transformation (4) because $\tilde X_\tau(\theta_0, v_0, r_0) \to (\theta^*, v^*, 0)$ as $\tau \to \infty$ iff the (θ, v) coordinates of the trajectory of (2) starting at $(\theta_0, v_0, -2\alpha^{-1}\ln r_0)$ tend to (θ^*, v^*) as $\tau \to \infty$. Thus we study the asymptotic behavior of (2) by studying the structure of the basins of the stable equilibria of (7), or, equivalently, the structure of the basin boundaries $\tilde W_n^s$, $n \in \mathbf{Z}$.

We summarize another approach to a particular case of (2) with exponentially decaying sinusoidal forcing. Varghese and Thorp (1988a) study basin boundaries of

$$(\dot\theta, \dot v, \dot t) = (v, -\sin\theta - dv + ge^{-\alpha t}\cos\omega t, 1), \qquad (\theta, v, t) \in \mathbb{R}^3, \tag{8}$$

by studying the 4-dimensional vector field

$$(\dot\theta, \dot v, \dot x_3, \dot x_4) = (v, -\sin\theta - dv + x_3, -\alpha x_3 + \omega x_4, -\omega x_3 - \alpha x_4). \tag{9}$$

Vector field (9) has sinks at $(2n\pi, 0, 0, 0)$ and type 1 saddles at $((2n+1)\pi, 0, 0, 0)$, $n \in \mathbf{Z}$. The basins of the sinks are separated by the smooth 3-dimensional stable manifolds of the saddles. Some of the trajectories of (9) correspond to trajectories of (8); in particular, initial conditions of (8) in $\Sigma_{t=0}$ correspond to initial conditions of (9) in the 2-dimensional slice of $\mathbb{R}^4$ with $x_3(0) = g$ and $x_4(0) = 0$. Varghese and Thorp (1988a) numerically integrated these initial conditions to show that the basin boundaries of (8) were truncated fractals for a suitable choice of g and α. Varghese and Thorp (1988a) also showed that the flow induced a diffeomorphism between the truncated fractal basin boundary in the slice of (9) corresponding to $\Sigma_{t=0}$ and the simpler basin boundaries in the slice of (9) corresponding to $\Sigma_{t=\tau}$ for τ large. Our coordinate change applies to (8) and yields a simpler approach than (9), albeit with some lack of smoothness.

3. Qualitative Structure of the Basin Boundary

The stable manifold theorem implies that $\tilde W_n^s$ is a C^1 immersed 2-dimensional submanifold of $\mathbb{R}^3$. An immersed stable manifold can be folded and stretched in such a way that portions of the surface accumulate on each other (e.g., McDonald et al. 1985; Dobson 1989b). That is, the intersection of an immersed stable manifold with an arbitrarily small neighborhood of $\mathbb{R}^3$ can be diffeomorphic to the intersection of an infinite number of planes with a ball. (Other structures in addition to the planes may also be present.) This intricacy of immersion occurs in stable manifolds with fractal structure. In contrast, a stable manifold embedded in $\mathbb{R}^3$ cannot accumulate on itself; the intersection of an embedded stable manifold with a sufficiently small neighborhood is diffeomorphic to the intersection of a single plane with a ball (e.g., Warner (1983), pp. 28–29). Thus an embedded stable manifold cannot be fractal.

In the Appendix we prove the following lemma.

Lemma 1. *$\tilde W_n^s$ is a C^1 embedded submanifold of $\mathbb{R}^3$.*

The proof of Lemma 1 constructs a neighborhood M of $((2n+1)\pi, 0, 0)$ such that $\tilde W_n^s \cap M$ is embedded in M. In particular, M consists only of the local stable manifold $\tilde W_{n\,\mathrm{loc}}^s \cap M$ (which is always embedded) and points that tend to a sink. The points that tend to a sink cannot be in $\tilde W_n^s$ and hence $\tilde W_n^s \cap M = \tilde W_{n\,\mathrm{loc}}^s \cap M$ is embedded in M. $\tilde W_n^s$ is constructed by applying the backward flow to $\tilde W_n^s \cap M$, and $\tilde W_n^s \cap M$ embedded in M implies that $\tilde W_n^s$ is embedded in $\mathbb{R}^3$.

Lemma 1 implies that $\tilde W_n^s$ is not fractal. It also follows from Lemma 1 that $\tilde W_n^s$ is closed and that $\tilde W_n^s$ is all of the basin boundary separating the basin of $(2n\pi, 0, 0)$ from the basin of $(2(n+1)\pi, 0, 0)$. (Fractally immersed basin boundaries are proper subsets of their closures, and the basin boundary is a closed set that must contain the closure of the stable manifold.)

We also study the intersection $\tilde{W}_n^s \cap \Sigma_{r=k}$ of the basin boundary with a plane of constant r coordinate. The structure of $\tilde{W}_n^s \cap \Sigma_{r=k}$ is of interest for several reasons. Since $\Sigma_{r=k}$ corresponds to initial conditions of (2) at a constant starting time, it is natural to study how $\tilde{W}_n^s \cap \Sigma_{r=k}$ is immersed in $\Sigma_{r=k}$. The simulation results in Varghese and Thorp (1988a) give some indication of how $\tilde{W}_n^s \cap \Sigma_{r=k}$ is immersed in $\Sigma_{r=k}$; they show that $\tilde{W}_n^s \cap \Sigma_{r=k}$ in a bounded subset of $\Sigma_{r=k}$ is a truncated fractal having seemingly disconnected striations. Our mathematical description of the immersion enables us to interpret the simulation results more fully. Also, it is easier to comprehend how $\tilde{W}_n^s \cap \Sigma_{r=k}$ is immersed in $\Sigma_{r=k}$ than it is to comprehend how $\tilde{W}_n^s$ is immersed in the state space $\mathbb{R}^2 \times \mathbb{R}$ because $\Sigma_{r=k}$ has one less dimension than the state space.

In the Appendix we prove a sequence of lemmas to arrive at Lemma 4:

Lemma 4. *$\tilde{W}_n^s \cap \Sigma_{r=k}$ is a C^1 embedding of $\mathbb{R}$ into $\Sigma_{r=k}$ for all $k \in \mathbb{R}$.*

In particular, Lemma 4 implies that $\tilde{W}_n^s \cap \Sigma_{r=k}$ is connected, which is by no means apparent from the simulation results of Varghese and Thorp (1988a).

The arguments leading to Lemma 4 are now summarized. First we show that $\tilde{W}_n^s$ intersects $\Sigma_{r=k}$ transversely (Lemma 2). This follows for nonzero k because the flow $\tilde{X}$ is transverse to $\Sigma_{r=k}$ and $\tilde{W}_n^s$ is invariant. Manifold intersection theory and the transversality of the intersection imply that $\tilde{W}_n^s \cap \Sigma_{r=k}$ is a C^1 1-dimensional embedded submanifold of $\Sigma_{r=k}$. We then prove that $\tilde{W}_n^s \cap \Sigma_{r=k}$ is connected and apply the classification theorem for 1-dimensional manifolds to conclude that $\tilde{W}_n^s \cap \Sigma_{r=k}$ is an embedding of either a circle or $\mathbb{R}$ in $\Sigma_{r=k}$. After eliminating the possibility that $\tilde{W}_n^s \cap \Sigma_{r=k}$ is an embedding of a circle in $\Sigma_{r=k}$, we conclude that $\tilde{W}_n^s \cap \Sigma_{r=k}$ is an embedding of $\mathbb{R}$ in $\Sigma_{r=k}$ (Lemma 4). These results rely on the r dynamics being independent of θ and v and on "straightening out" $\tilde{W}_n^s$ into a hyperplane in a neighborhood of W_n^s with a coordinate change that preserves the r coordinate (Lemma 3).

Despite the lemmas, the basin boundary can have a complicated, truncated fractal structure. For example, consider (2) with a constant amplitude sinusoidal forcing of period T for negative time and sinusoidal forcing with exponentially decaying amplitude for positive time. For negative time the system is periodic and can be studied with a Poincaré map $P = \tilde{X}_{-T}$ on the Poincaré section $\Sigma_{t=0}$. For small forcing amplitude and damping, P has a hyperbolic saddle fixed point γ_0 near $((2n+1)\pi, 0)$. We choose the amplitude of the forcing for negative time large enough relative to the damping so that P has a fractal basin boundary $\overline{W^s(\gamma_0)}$ (Guckenheimer and Holmes 1986; Hockett and Holmes 1986; Dobson 1989b). We expect $\tilde{W}_n^s \cap \Sigma_{t=0}$ to intersect the Poincaré map unstable manifold $W^u(\gamma_0)$ transversely and it follows from the lambda lemma (Guckenheimer and Holmes 1986) that portions of $\tilde{W}_n^s \cap \Sigma_{-mT} = P^m(\tilde{W}_n^s \cap \Sigma_{t=0})$ tend to the fractal $\overline{W^s(\gamma_0)}$ as m tends to infinity. Thus $\tilde{W}_n^s \cap \Sigma_{t=\tau}$ is a truncated fractal of increasing complexity as τ tends to $-\infty$. It is consistent for $\tilde{W}_n^s$ to be an embedded submanifold and to be "asymptotically fractal" as time tends to $-\infty$. (Fractal basin boundaries require an infinite time to evolve (Dobson 1989b) and $\tilde{W}_n^s \cap \Sigma_{t=\tau}$ is not fractal because it has only evolved for a finite time.)

4. Example: Impulsive Forcing at Time Zero

One instructive special case assumes forcing that is zero for negative time. The basin boundary at time $\tau < 0$ can then be determined by integrating the basin boundary at time zero backward for time $|\tau|$. Since the forcing is off during this period, the vector field integrated backward is just that of the unforced pendulum, and it is therefore easy to observe the folding and stretching of the boundary during the backward integration. In fact, the asymptotic behavior as τ tends to $-\infty$ is specified completely within a bounded region by the intersections of the basin boundary at time zero with the unstable manifolds W_m^u, $m \in \mathbf{Z}$, of the saddles of the unforced pendulum. Much of the possible complexity of the basin boundary is due to the fact that a single connected basin boundary at time zero can tend to several of the stable manifolds of the unforced pendulum as time tends to $-\infty$.

We present the case of a pendulum forced by a single impulse at time zero to show by elementary methods how the folding and stretching of the boundary may arise. In particular, this example can exhibit tongues and striations similar to those occurring in the more analytically difficult case studied with simulation by Varghese and Thorp (1988a). We show the effect of an impulsive forcing $f(t) = g\delta(t)$ at time zero for various forcing strengths g to illustrate how different possible qualitative behaviors depend on the intersections of $\tilde{W}_n^s \cap \Sigma_{t=0}$ with W_m^u, $m \in \mathbf{Z}$. (We write δ for the unit impulse.) One advantage of considering impulsive forcing is that the effect of the forcing on $\tilde{W}_n^s \cap \Sigma_{t=0}$ is easy to work out; the forcing simply moves $\tilde{W}_n^s \cap \Sigma_{t=0}$ in the v direction by a distance g. (An objection to considering impulsive forcing is that δ is not a smooth function as assumed in Section 1. However the results that follow also apply to smooth approximations to δ.)

The conventions for Figures 1–5 are as follows: The representation is qualitative. The equilibria shown are of the unforced pendulum flow X with a horizontal θ-axis and a vertical v-axis. The left hand saddle is at $(-\pi, 0)$, the spiral sink is at $(0, 0)$ and the right hand saddle is at $(\pi, 0)$. The thick solid lines show the stable manifolds W_0^s, W_{-1}^s and unstable manifolds W_0^u, W_{-1}^u of the saddles. The dashed lines show $\tilde{W}_0^s \cap \Sigma_{t=0-}$, the basin boundary just before the perturbation. The thin solid lines show $\tilde{W}_0^s \cap \Sigma_{t=\tau}$ for τ negative and large in magnitude. After the perturbation the basin boundary is identical to W_0^s.

If g is small, then $\tilde{W}_0^s \cap \Sigma_{t=0-}$ intersects only W_0^u as shown in Figure 1 and backward integration yields $\tilde{W}_0^s \cap \Sigma_{t=\tau}$ close to W_0^s. In fact, all the points of $\tilde{W}_0^s \cap \Sigma_{t=\tau}$ except the intersection with W_0^u tend to infinity as τ tends to $-\infty$. However, the part of $\tilde{W}_0^s \cap \Sigma_{t=\tau}$ remaining in any given bounded set becomes C^1 close to W_0^s as τ tends to $-\infty$. (This is an application of the lambda lemma (Guckenheimer and Holmes 1986).) Thus a small impulse perturbs the basin boundaries a little but they tend back to their unperturbed positions.

If g is large enough relative to the damping d so that $\tilde{W}_0^s \cap \Sigma_{t=0-}$ also intersects W_{-1}^u as shown in Figure 2, then the position of $\tilde{W}_0^s \cap \Sigma_{t=\tau}$ in Figure 2 shows how $\tilde{W}_0^s \cap \Sigma_{t=\tau}$ tends to W_0^s and W_{-1}^s as $\tau \to -\infty$. In addition to a segment of $\tilde{W}_0^s \cap \Sigma_{t=\tau}$ tending to W_0^u as in the case for small g, there is a long thin "finger" that tends to W_{-1}^s. Further backward integration of $\tilde{W}_0^s \cap \Sigma_{t=\tau}$ yields in the bounded area shown in Figure 2 two thin solid lines close to W^s_{-1} and one thin solid line close to W^s_0, the connections between these lines having left the bounded area of the figure as they tend to infinity. Thus although $\tilde{W}^s_0 \cap \Sigma_{t=\tau}$ is always a connected curve, it may appear disconnected on a bounded set because the connecting portions tend to infinity (compare the simulation results of Varghese and Thorp (1988a)).

The effects of successively larger values of g are shown in Figures 3 and 4. The higher number of intersections between $\tilde{W}^s_0 \cap \Sigma_{t=0-}$ and W^u_0 and W^u_{-1} causes $\tilde{W}^s_0 \cap \Sigma_{t=\tau}$ to "wind" around the figure several times staying close to W^s_0 and W^s_{-1}. The winding of $\tilde{W}^s_0 \cap \Sigma_{t=\tau}$ is caused by the basin of the spiral sink unwinding in backward time. As the number of intersections between $\tilde{W}^s_0 \cap \Sigma_{t=0-}$ and W^u_0 and W^u_{-1} grows, so does the number of times $\tilde{W}^s_0 \cap \Sigma_{t=\tau}$ winds around.

Note that at time τ there is a sizable region around the sink of the unforced pendulum at $(0, 0)$ that remains in a single basin of the forced pendulum. This follows because the basin boundaries are close to W^s_0 and W^s_{-1} at time τ and are

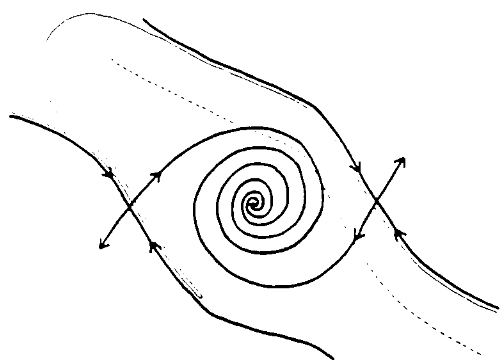

Fig. 2. A larger impulse.

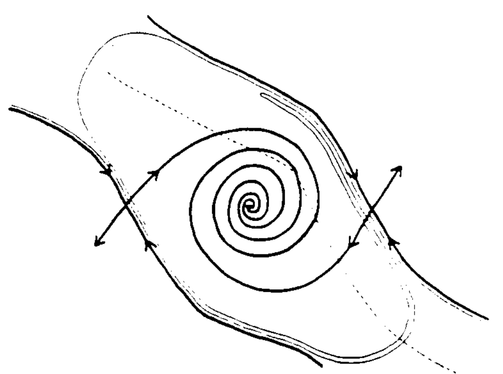

Fig. 3. A yet larger impulse.

bounded away from the sink. However, Figures 2 and 3 differ from Figure 4 since the region lies in the basins of different sinks of the forced pendulum. In Figures 2 and 3 trajectories starting near $(0, 0)$ at a negative time are in the basin of the sink $(\theta, v, t) = (0, 0, \infty)$ (this sink is more properly labeled $(\theta, v, r) = (0, 0, 0)$). Thus if the pendulum is operated near the sink it will not be dislodged from the basin of that sink by the impulse. On the other hand, in Figure 4 trajectories starting near $(0, 0)$ at a negative time are in the basin of the sink $(\theta, v, t) = (2\pi, 0, \infty)$ since the impulse is large enough to push these trajectories into the basin of attraction of that sink.

Figure 5 shows an exceptional case that represents the transition from the situation of Figure 3 to that of Figure 4. g is adjusted so that $\tilde{W}^s_0 \cap \Sigma_{t=0-}$ passes through $(\theta, v, t) = (0, 0, 0)$. In this case, the basin boundary winds around forever as time tends to $-\infty$ and every neighborhood of $(0, 0, s)$, $s < 0$, intersects a basin boundary

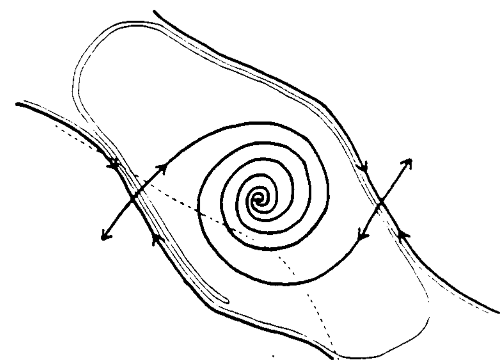

Fig. 4. A very large impulse.

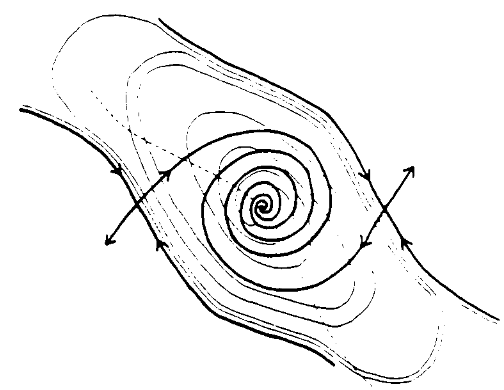

Fig. 5. An exceptional case between Figures 3 and 4.

and two basins. The effects of this particular forcing are not confined to increasingly small strips near W_m^s, $m \in \mathbf{Z}$, as time tends to $-\infty$.

We have considered the pendulum forced with an impulse by studying basin *boundaries* as they evolve in backward time. The phenomena can also be understood from the point of view of the basins evolving in backward time or trajectories in forward time. The approach using basins rather than basin boundaries evolving in backward time requires a slight shift in perception, but is worth describing. The effect of the backward integration in Figure 2 can be perceived as grasping a small area of the basin of $(2\pi, 0, \infty)$ at time zero and stretching it out into a long finger by time τ. (Think of the basins as made of putty.)

The basin boundary at time τ in Figure 2 can be discussed in terms of trajectories. Most trajectories starting at time τ in the basin of $(0, 0)$ for the unforced pendulum are in the basin of $(0, 0, \infty)$ for the forced pendulum. Since τ is a negative time of large magnitude, most such trajectories move close enough to the sink before the impulse at time zero so that they are not perturbed into the next basin. However, since trajectories can take an arbitrarily long time to pass close to a saddle, trajectories near W_0^s and W_{-1}^s may take so long to pass their saddle that they arrive sufficiently far from the sink at time $0-$ for the impulse to perturb them to the next basin. This explains why the basin boundaries at time τ are usually so close to W_0^s and W_{-1}^s.

We remark that a pendulum forced with a periodic series of impulses of equal strength but alternating sign can be analyzed in a similar manner to the example above so that the formation of a true fractal basin boundary can be observed using elementary methods.

5. Perturbation Methods

The stable manifolds comprising the basin boundaries may be constructed by perturbation methods if different assumptions are made on the forcing function f. The new assumptions on f are that the conditions (3) on the size and rate of decay of f are replaced by the condition that f is smooth and sufficiently C^1 small.

The vector field

$$(\dot\theta, \dot v, \dot t) = (v, -\sin\theta - dv, 1), \qquad (\theta, v, t) \in \mathbb{R}^3, \tag{10}$$

is the time suspension of the damped, unforced pendulum (1). Vector field (10) has uniformly hyperbolic orbits $((2n+1)\pi, 0) \times \mathbb{R}$, $n \in \mathbf{Z}$. (Anosov (1967) and Lerman and Shil'nikov (1992) refer to the uniformly hyperbolic property as an exponential dichotomy of solutions.) The orbits $((2n+1)\pi, 0) \times \mathbb{R}$ have the cylindrical stable manifolds $W_n^s \times \mathbb{R}$. Then a version of the Hadamard–Perron theorem (Anosov 1967) proves that this structure is preserved when the small forcing f is included. That is, there is an orbit of the perturbed system (2) C^1 close to $((2n+1)\pi, 0) \times \mathbb{R}$ which has a stable manifold. If the conditions (3) on the decay of f are also satisfied, then this stable manifold must correspond to the stable manifold $\tilde W_n^s$ constructed above.

6. Conclusions

We study the qualitative properties of basin boundaries for the pendulum with nonperiodic forcing. The forcing is assumed to be smooth and have its norm and the norm of its derivative bounded asymptotically by an exponential decay, but is otherwise unrestricted. We present a time coordinate change that allows the basin boundaries to be identified with the 2-dimensional stable manifolds $\tilde W_n^s$, $n \in \mathbf{Z}$, of hyperbolic equilibria in the middle of a 3-dimensional state space. This transformation allows us to apply dynamical systems techniques to study the basin boundaries. In particular, the basin boundaries are C^1 embedded submanifolds and hence cannot be true fractals. However, the example in Section 3 and the simulation results of Varghese and Thorp (1988a) show that the basin boundaries can be truncated fractals. The complexity of these basin boundaries shows the difficulty of devising general means of calculating basin boundaries even in low dimensional examples. It is natural to study the intersection $\tilde W_n^s \cap \Sigma_{t=\tau}$ of the basin boundary $\tilde W_n^s$ with a state space time slice $\Sigma_{t=\tau}$ of constant initial time τ. $\tilde W_n^s \cap \Sigma_{t=\tau}$ is a C^1 embedding of $\mathbb{R}$ in $\Sigma_{t=\tau}$. In particular $\tilde W_n^s \cap \Sigma_{t=\tau}$, which may appear disconnected in simulations (Varghese and Thorp 1988a), is in fact connected. The intricate stretching and folding of the basin boundary for some forcings can be attributed to stretching and folding of $\tilde W_n^s \cap \Sigma_{t=\tau}$ within the time slice as time τ changes. The tongues and striations arising in the simulations of Varghese and Thorp (1988a) also arise in the much simpler setting of the impulsively forced pendulum, and their formation is more transparent in that context. The time coordinate transformation of the forced pendulum yields both analytic and conceptual benefits. It allows the qualitative nature of the basin boundary to be analyzed rigorously for a general class of forcing, and permits the formation of complicated basin boundaries to be understood more simply for particular types of forcing.

Appendix

Lemma 1. *$\tilde W_n^s$ is a C^1 embedded submanifold of $\mathbb{R}^3$.*

Proof. We begin by using the stable manifold theorem to construct the local stable manifold $W_{n\,\mathrm{loc}}^s$ in a neighborhood M_1 of $((2n+1)\pi, 0, 0)$. The construction (Palis and DeMelo 1982, Proposition 6.1 and Theorem 6.2) ensures that $W_{n\,\mathrm{loc}}^s$ is C^1 embedded in M_1.

Now we restrict our attention to the vector field X on $\Sigma_{r=0}$. X is given by $X(\theta', v) = (v, \sin\theta' - dv)$, where θ' is the coordinate $\theta' = \theta - (2n+1)\pi$. We construct a closed parallelogram A in $M_1 \cap \Sigma_{r=0}$ containing $((2n+1)\pi, 0, 0)$ with edges transverse to X. The edges of A are perpendicular to the eigenvectors $(-\lambda_1, 1)$, $(-\lambda_2, 1)$ of $DX|_{(0,0)}$ so that the flow of $DX|_{(0,0)}$ is transverse to the edges of A. If A is sufficiently small, X is sufficiently close to $DX|_{(0,0)}$ in A and is also transverse to the edges of A. The details of the construction of A follow:

The eigenvalues of $DX|_{(0,0)}$ satisfy $\lambda^2 + d\lambda - 1 = 0$ and are $\lambda_1 = -d/2 + \sqrt{1 + d^2/4}$ and $\lambda_2 = -d/2 - \sqrt{1 + d^2/4}$. The edges of A, $\partial A_\pm^1$ and $\partial A_\pm^2$ are determined by the straight lines $-\lambda_1\theta' + v = \pm\eta$ and $-\lambda_2\theta' + v = \pm\eta$, respectively. X is transverse to

$\partial A^2_{\mp}$ for sufficiently small η because

$$\begin{aligned} X \cdot (-\lambda_1, 1) &= -(\lambda_1 + d)v + \sin\theta' \\ &= \lambda_2(v - \lambda_1\theta') + \sin\theta' - \theta' \\ &= \pm\lambda_2\eta + \sin\theta' - \theta', \end{aligned} \tag{11}$$

which is bounded away from zero by a constant times η for sufficiently small η. Note that $\lambda_2 \neq 0$ because the damping $d > 0$ and that $\sin\theta' - \theta'$ is $O(\eta^3)$ (the corners of A have coordinates proportional to η so that $(\theta', v) \in A$ implies that $\theta', v \leq K\eta$ for fixed K). Also note that the transversality is uniform along $\partial A^2_{\pm}$ in the sense that $X \cdot (\lambda_1, 1)$ is uniformly bounded away from zero. Interchanging λ_1 and λ_2 in equation (11) shows that X is transverse to $\partial A^1_{\pm}$ for small η. Moreover, X leaves A through $\partial A^2_{\pm}$ and enters A through $\partial A^1_{\pm}$.

Now reduce the size of η (if necessary) to ensure that all of the trajectories leaving through $\partial A^2_{\pm}$ approach a sink (it is evident from the phase portrait of X that this is possible since the damping $d > 0$) and also to ensure that $A \subset M_1 \cap \Sigma_{r=0}$.

We return to the 3-dimensional vector field $\tilde{X}$ and define the parallelepiped $\tilde{A} = \{(\theta', v, r) \mid (\theta', v) \in A, |r| \leq \rho\}$. Choose ρ small enough that $\tilde{A} \subset M_1$ and:

1. $\tilde{X}$ is transverse to $\partial\tilde{A}^1_{\pm}$ and $\partial\tilde{A}^2_{\mp}$, the vertical sides of $\tilde{A}$ corresponding to the edges $\partial A^1_{\pm}$ and $\partial A^2_{\mp}$ of A. (This condition can be satisfied because transversality is preserved under small perturbations and X is uniformly transverse to $\partial A^1_{\pm}$ and $\partial A^2_{\mp}$.)
2. $\partial\tilde{A}^2_{\mp}$ is contained in the basin of a sink. (This condition can be satisfied because $\partial\tilde{A}^2_{\mp}$ is contained in a neighborhood of $\partial A^2_{\pm}$, a closed interval contained in the basin of a sink.)

$\tilde{X}$ is transverse to $\Sigma_{r=\pm\rho}$ because $\dot{r}$ is nonzero except on $\Sigma_{r=0}$ and in fact $\tilde{X}$ enters $\tilde{A}$ through $\tilde{A} \cap \Sigma_{r=\pm\rho}$. Since $\tilde{X}$ also enters $\tilde{A}$ through $\partial\tilde{A}^1_{\pm}$, any trajectory leaving $\tilde{A}$ must leave through $\partial\tilde{A}^2_{\mp}$ and tend to a sink. Thus points in $\tilde{A}$ either have trajectories staying in $\tilde{A}$, in which case they are in $\tilde{W}^s_{n\,\mathrm{loc}}$ and tend to $((2n+1)\pi, 0, 0)$ or they leave $\tilde{A}$ and tend to a sink and are not in $\tilde{W}^s_n$. Therefore $\tilde{W}^s_n \cap \tilde{A} = \tilde{W}^s_{n\,\mathrm{loc}} \cap \tilde{A}$. Choose M to be a neighborhood of $((2n+1)\pi, 0, 0)$ contained in $\tilde{A}$. Then $\tilde{W}^s_n \cap M = \tilde{W}^s_{n\,\mathrm{loc}} \cap M$ and since $\tilde{W}^s_{n\,\mathrm{loc}} \cap M$ is C^1 embedded in M, $\tilde{W}^s_n \cap M$ is C^1 embedded in M.

Since $\tilde{W}^s_n = \bigcup\{\tilde{X}_{-\tau}(\tilde{W}^s_n \cap M) \mid \tau \geq 0\}$, there is a neighborhood N in $\mathbb{R}^3$ of each point in $\tilde{W}^s_n$ that is diffeomorphic by the flow to a neighborhood in M of a point in $\tilde{W}^s_n \cap M$, and $\tilde{W}^s_n \cap N$ is therefore embedded in N. Hence $\tilde{W}^s_n$ is C^1 embedded in $\mathbb{R}^3$. □

Lemma 2. *$\tilde{W}^s_n$ has a nonempty transversal intersection with $\Sigma_{r=k}$ for all $k \in \mathbb{R}$.*

Proof. First prove the lemma for $k = 0$. $\tilde{W}^s_n \cap \Sigma_{r=0} = W^s_n$ and is nonempty. $\tilde{W}^s_n$ intersects $\Sigma_{r=0}$ transversely near $((2n+1)\pi, 0, 0)$ since the eigenvector corresponding to $\dot{r} = -\alpha r/2$ is normal to $\Sigma_{r=0}$. The backward flow $\tilde{X}_{-t}$ extends this transversal intersection near $((2n+1)\pi, 0, 0)$ to a transversal intersection of $\tilde{W}^s_n$ and $\Sigma_{r=0}$ along all of W^s_n. There is a $\rho > 0$ such that $\tilde{W}^s_n \cap \Sigma_{r=\rho}$ is nonempty because of the openness of transversality. Backward integration of $\tilde{W}^s_n \cap \Sigma_{r=\rho}$ for time $k - \rho$ shows that $\tilde{W}^s_n \cap \Sigma_{r=k}$ is nonempty for any positive $k \in \mathbb{R}$ and the argument for negative k is similar. $\tilde{W}^s_n$ intersects $\Sigma_{r=k}$ transversely for $k \neq 0$ because $\tilde{X}$ is transverse to $\Sigma_{r=k}$ for $k \neq 0$ and $\tilde{W}^s_n$ is invariant. □

Lemma 3. *There is a C^1 diffeomorphism preserving the r coordinate and making $\tilde{W}^s_n$ a hyperplane in a neighborhood B of $((2n+1)\pi, 0, 0)$.*

Proof. The proof uses a standard technique from Warner (1983, Proposition 1.35). W^s_n is a smooth embedding σ of $\mathbb{R}$ in $\mathbb{R}^3$ and it is easy to check that $\theta\sigma\colon \mathbb{R} \to \mathbb{R}$ is regular. Define a new coordinate system for $\mathbb{R}^3$ by $(\theta', v', r') = (\theta, v - v\sigma(\theta\sigma)^{-1}\theta, r)$. The coordinate change is a diffeomorphism since $dv' = dv - d(v\sigma(\theta\sigma)^{-1})\,d\theta$ implies that the Jacobian is invertible and since for given θ, v' is a monotonic and hence globally invertible function of v.

W^s_n is the straight line $v' = r' = 0$ in the dashed coordinates ($v'\sigma = v\sigma - v\sigma = 0$). It follows that the vector $(0, 1, 0)$ (in the dashed coordinates) is everywhere transverse to W^s_n. Since $\tilde{W}^s_n$ is a surface intersecting $\Sigma_{r=0}$ transversely at W^s_n (Lemma 2), $(0, 1, 0)$ is transverse to $\tilde{W}^s_n$ everywhere on W^s_n. Thus if we write ϕ for the C^1 immersion $\mathbb{R}^2 \to \mathbb{R}^3$ whose image is $\tilde{W}^s_n$ (see Palis and de Melo (1982, Section 2.6)) and π for the projection $(\theta', v', r') \mapsto (\theta', r')$ onto $\mathbb{R}^2$, then $\pi\phi$ is regular on $\phi^{-1}(W^s_n)$. Lemma 1 implies that ϕ is a C^1 embedding.

There is a neighborhood M of $\phi^{-1}(W^s_n)$ in $\mathbb{R}^2$ such that $\pi\phi$ is regular on M. Since ϕ is an embedding, $\phi(M)$ is open in the induced topology on $\tilde{W}^s_n$ and there is a neighborhood B of $\phi(M)$ in $\mathbb{R}^3$ such that $B \cap \tilde{W}^s_n = \phi(M)$. Change coordinates in B according to $(\theta'', v'', r'') = (\theta', v' - v'\phi(\pi\phi)^{-1}\pi, r')$. This coordinate change also has an invertible Jacobian and is a diffeomorphism if B is shrunk as required. In the dashed coordinates on B, $\tilde{W}^s_n \cap N$ is given by the hyperplane $v'' = 0$. Note that both coordinate changes are C^1 diffeomorphisms and preserve the r coordinate. □

Lemma 4. *$\tilde{W}^s_n \cap \Sigma_{r=k}$ is a C^1 embedding of $\mathbb{R}$ into $\Sigma_{r=k}$ for all $k \in \mathbb{R}$.*

Proof. Lemmas 1 and 2 imply that $\tilde{W}^s_n$ and $\Sigma_{r=k}$ are C^1 embedded 2-dimensional submanifolds of $\mathbb{R}^3$ with nonempty transversal intersection. It follows that $\tilde{W}^s_n \cap \Sigma_{r=k}$ is a C^1 embedded 1-dimensional submanifold of $\Sigma_{r=k}$ (Warner 1983, Theorem 1.39).

Now we show that $\tilde{W}^s_n \cap \Sigma_{r=k}$ is path connected. Choose the neighborhood B of $((2n+1)\pi, 0, 0)$ in Lemma 3 so that it is a ball in the new coordinates of Lemma 3. Choose $x, y \in \tilde{W}^s_n \cap \Sigma_{r=k}$. There exists $T \in \mathbb{R}$ such that $\tilde{X}_T(x), \tilde{X}_T(y) \in B$. Moreover, since the r dynamics do not depend on θ and v, $\tilde{X}_T(x), \tilde{X}_T(y) \in B \cap \Sigma_{r=\rho}$, where $\rho = e^{-\alpha T/2}k$. The coordinate change of Lemma 3 preserves $\Sigma_{r=\rho}$ and makes $\tilde{W}^s_n \cap B$ a plane and B convex. Hence there is a path in $\tilde{W}^s_n \cap \Sigma_{r=\rho} \cap B$ joining $\tilde{X}_T(x)$ and $\tilde{X}_T(y)$. The image under $\tilde{X}_{-T}$ of this path is a path in $\tilde{W}^s_n \cap \Sigma_{r=k}$ joining x and y.

Since $\tilde{W}^s_n \cap \Sigma_{r=k}$ is a connected and C^1 embedded 1-dimensional submanifold, the classification theorem for one-manifolds (Milnor (1981)) shows that $\tilde{W}^s_n \cap \Sigma_{r=k}$ is an embedding either of $\mathbb{R}$ or of S^1 into $\Sigma_{r=k}$. However, if $\tilde{W}^s_n \cap \Sigma_{r=k}$ were an embedding of S^1 into $\Sigma_{r=k}$, then it would be compact and there would exist a time $T \in \mathbb{R}$ such that $\tilde{X}_T(\tilde{W}^s_n \cap \Sigma_{r=k}) \subset \tilde{W}^s_n \cap \Sigma_{r=\rho} \cap B$. However, $\tilde{W}^s_n \cap B$ is a plane in the coordinates of Lemma 3 and so $\tilde{W}_n^s \cap \Sigma_{r=\rho} \cap B$ is a line segment, implying that $\tilde{X}_T$ would be a diffeomorphism mapping S^1 into a line segment, which is impossible. Therefore, $\tilde{W}_n^s \cap \Sigma_{r=k}$ is a C^1 embedding of $\mathbb{R}$ into $\Sigma_{r=k}$. □

Acknowledgments

We thank M. Varghese and J. S. Thorp for useful discussions. We thank Steve Wiggins and an anonymous reviewer for suggestions and references on perturbation theory. This research was supported in part by the National Science Foundation under grants ECS-83-52211 and ECS-91-57192 and by the Army Research Office through the Mathematical Sciences Institute at Cornell University.

References

Anosov, D. V. (1967): Geodesic flows on closed Riemann manifolds with negative curvature. Proceedings of the Steklov Institute of Mathematics, no. 90. English translation, American Mathematical Society, Providence, RI, 1969.
Dobson, I. (1989a): Describing complicated basin boundaries in a forced oscillator. Ph.D. thesis, Cornell University, Ithaca NY 14853, May, Chapter 5.
Dobson, I. (1989b): Formation of a fractal basin boundary in a forced oscillator. IEEE Transactions on Circuits and Systems, vol. 36, no. 6, June, pp. 866–872.
Dobson, I., Delchamps, D. F. (1989): Basin boundaries in the pendulum with nonperiodic forcing. Proceedings of the 23rd Annual Conference on Information Science and Systems, Baltimore, MD, March, pp. 374–379.
Grebogi, C., McDonald, S. W., Ott, E., Yorke, J. A. (1983): Final state sensitivity: an obstruction to predictability. Physics Letters A, vol. 99, no. 9, December, pp. 415–418.
Grebogi, C., Ott, E., Yorke, J. A. (1987): Basin boundary metamorphoses: Changes in accessible boundary orbits. Physica D, vol. 24, pp. 243–262
Guckenheimer, J., Holmes, P. (1986): Nonlinear Oscillations, Dynamical Systems and Bifurcations of Vector Fields. Springer-Verlag, New York.
Gwinn, E. G., Westervelt, R. M. (1985): Intermittent chaos and low frequency noise in the driven damped pendulum. Physical Review Letters, vol. 54, no. 15, April, pp. 1613–1616.
Hammel, S. M., Jones, C. K. R. T. (1989): Jumping stable manifolds for dissipative maps of the plane. Physica D, vol. 35, pp. 87–106.
Hockett, K., Holmes, P. (1986): Josephsons junction, annulus maps, Birkhoff attractors, horseshoes and rotation sets. Ergodic Theory Dynamical Systems, vol. 6, pp. 205–239.
Lerman, L. M., Shil'nikov, L. P. (1992): Homoclinical structures in nonautonomous systems: nonautonomous chaos. Chaos, vol. 2, no. 3, pp. 447–454.
McDonald, S. W., Grebogi, C., Ott, E., Yorke, J. A. (1985): Fractal basin boundaries. Physica D, vol. 17, pp. 125–153.
Milnor, J. W. (1981): Appendix to Topology from the Differentiable Viewpoint, The University Press of Virginia, Charlottesville.
Moon, F. C., Li, G-X. (1985): Fractal basin boundaries and homoclinic orbits for periodic motion in a two well potential. Physical Review Letters, vol. 55, no. 14, September, pp. 1439–1442.
Palis, J., de Melo, W. (1982): Geometric Theory of Dynamical Systems; An Introduction. Springer-Verlag, New York.
Varghese, M., Thorp, J. S. (1988a): Truncated-fractal basin boundaries in forced pendulum systems. Physical Review Letters, vol. 60, no. 8, February, pp. 665–668.
Varghese, M., Thorp, J. S. (1988b): An analysis of truncated fractal growths in the stability boundaries of three-node swing equations. IEEE Transactions on Circuits and Systems, vol. CAS-35, no. 7, July, pp. 825–834.
Warner, F. W. (1983) Foundations of Differentiable Manifolds and Lie Groups. Scott, Foresman and Co., 1971 or Springer-Verlag, New York, 1983.

J. Nonlinear Sci. Vol. 4: pp. 329–354 (1994)

Journal of Nonlinear Science

Transport in 3D Volume-Preserving Flows

R. S. MacKay
Nonlinear Systems Laboratory, Mathematics Institute, University of Warwick, Coventry CV4 7AL, UK

Received January 26, 1993; revised manuscript accepted for publication October 18, 1993
Communicated by Stephen Wiggins

Summary. The idea of surfaces of locally minimal flux is introduced as a key concept for understanding transport in steady three-dimensional, volume-preserving flows. Particular attention is paid to the role of the skeleton formed by the equilibrium points, selected hyperbolic periodic orbits and cantori and connecting orbits, to which many surfaces of locally minimal flux can be attached. Applications are given to spheromaks (spherical vortices) and eccentric Taylor–Couette Flow.

Key words. volume-preserving flows, skeleton, locally minimal flux, sneaky returns

AMS Subject Classifications. 58F11

1. Introduction

What is the fraction of the fluid originally in a region R_1 which is in region R_2 at time t? This is the basic transport question. It is non-trivial to answer even for steady flows. It is a question of considerable importance for applications where mixing is desired, or where it is to be minimised.[1]

In this paper I review some standard notions for volume-preserving flows and introduce some new ideas. All the concepts are illustrated by application to two important examples.

The mathematical framework to be taken is that of a steady C^1 divergence-free vector field $\mathbf{u}(\mathbf{x})$ in a 3D region Ω. The principal example is the velocity field for an incompressible fluid flow. The same mathematics also applies, however, to the mass flux $\mathbf{J} = \rho\mathbf{u}$ for a steady compressible fluid flow $\mathbf{u}$ with density $\rho(\mathbf{x})$, the vorticity field $\boldsymbol{\omega} = \text{curl}\,\mathbf{u}$ of a fluid flow $\mathbf{u}$, a magnetic field $\mathbf{B}$, a steady current field, $\mathbf{j}$, the vector

[1] Note, however, that mixing and transport are not synonyms. Mixing depends on small-scale stretching (Lyapunov exponents), whereas transport has to do with large-scale movement.